Available online at www.eccomasproceedia.org
Eccomas Proceedia COMPDYN (2017) 3795-3807

ECCOMAS
Proceedia

COMPDYN 2017
6th ECCOMAS Thematic Conference on
Computational Methods in Structural Dynamics and Earthquake Engineering
M. Papadrakakis, M. Fragiadakis (eds.)
Rhodes Island, Greece, 15–17 June, 2017

NUMERICAL ANALYSIS OF FLUTTER INSTABILITY IN SIMPLIFIED BLADE CASCADE

Jan Vimmr[1], Ondřej Bublík[1], Aleš Pecka[1], and Luděk Pešek[2]

[1]European Centre of Excellence NTIS - New Technologies for the Information Society,
Faculty of Applied Sciences, University of West Bohemia
Univerzitní 8, Pilsen, CZ-306 14, Czech Republic
e-mail: jvimmr@kme.zcu.cz, {obublik, pecka}@ntis.zcu.cz

[2] Institute of Thermomechanics AS CR, v.v.i., Academy of Sciences of the Czech Republic
Dolejškova 1402/5, Prague, CZ-182 00, Czech Republic
e-mail: pesek@it.cas.cz

Keywords: simplified blade cascade, flutter assessment, ALE formulation, discontinuous Galerkin method, aerodynamic damping parameter, travelling wave mode

Abstract. *In this paper the occurrence of flutter in a simplified blade cascade is analysed. The simplified blade cascade is formed by three flat plates, which perform a kinematic harmonic motion, each with a different inter-blade phase angle. The inter-blade phase angles are chosen in order for travelling wave mode of vibration to be present. The aim of the simulations is to determine the aerodynamic damping coefficients caused by the aerodynamic forces acting on the flat plates, which show whether flutter occurs. The non-linear system of Favre-averaged Navier-Stokes equations in ALE formulation completed by the Spalart-Allmaras turbulence model was chosen as the mathematical model. The simulations were performed using the developed in-house CFD software based on the discontinuous Galerkin method, which offers high order of accuracy.*

Peer-review under responsibility of the organizing committee of COMPDYN 2017.
doi: 10.7712/120117.5685.17525

1 INTRODUCTION

In the forties of the 20th century, first papers focused on the aero-elasticity of blades in axial turbines appeared, e.g. [1]. An empirical criterion for the presence of flutter based on a reduced blade frequency for bending blade vibration was introduced in [2]. The criterion states that if the reduced blade frequency is less than 0.33, the flutter is not excited. However, other influences such as geometric configuration of blade cascade and angle of attack can influence the occurrence of flutter. The problem of aero-elasticity is still a subject of interest since modern turbines are designed to withstand high operational temperatures and flow rates [3].

Originally, the term flutter was established for flow attached to the vibration of blade when phase displacement between blade motion and induced aerodynamic forces occurs. Depending on the time shift between the moving structure and unsteady aerodynamic forces acting on the structure, following cases can occur:

i) the kinetic energy of the blade is absorbed by the flow,

ii) the kinetic energy of the flow is transmitted to the blade.

In the first case, we talk about damped vibration from the aero-elasticity point of view. In the second case, the extra energy added to the blades results in the increase of amplitudes, in other words in unstable vibration, which we call flutter. It has been shown, see [4], that the critical flutter point, i.e. the highest aero-dynamical excitation, arises for a particular inter-blade phase angle. Most aerodynamic studies are based on the so called travelling wave mode of vibration, where one assumes that all blades vibrate at the same frequency, amplitude and inter-blade phase angle. Other aerodynamic studies use the influence coefficient technique which is based on calculating the aerodynamic forces of vibrating blade acting on non-vibrating adjacent blades.

For the purpose of this study, we choose the travelling wave mode approach. Following [4] we consider an unsteady flow through a simplified blade cascade formed by three flat plates. All the flat plates in the cascade perform a harmonic motion with given inter-blade phase angles so that their mutual movement creates travelling waves. In our paper [5], this problem was solved only for one inter-blade phase angle. The aim of this numerical study is to evaluate aerodynamic forces acting on the flat plates in the simplified cascade for the whole range of the inter-blade phase angles from $-\pi$ to π. Furthermore, the aerodynamic damping parameter is calculated out of the aerodynamic forces on which basis it is inferred whether flutter occurs. The upcoming simulations are performed using the developed in-house CFD software based on the discontinuous Galerkin method. The in-house CFD software is validated on two test problems described in section 4. In section 5 we present numerical results of unsteady compressible viscous fluid flow through the simplified blade cascade for various inter-blade phase angles.

2 MATHEMATICAL MODEL

A two-dimensional compressible viscous fluid flow in a time-varying computational domain $\Omega(t) \in \mathcal{R}^2$ with boundary $\partial\Omega$ is described by the non-linear system of Favre-averaged Navier-Stokes equations which, in the dimensionless arbitrary Lagrangian-Eulerian (ALE) formulation,

can be written as

$$\begin{aligned}
&\frac{D^A\bar{\varrho}}{Dt}+\frac{\partial(\bar{\varrho}\tilde{u}_j)}{\partial x_j}-U_j\frac{\partial\bar{\varrho}}{\partial x_j}=0,\\
&\frac{D^A}{Dt}(\bar{\varrho}\tilde{u}_i)+\frac{\partial}{\partial x_j}(\bar{\varrho}\tilde{u}_i\tilde{u}_j+\bar{p}\delta_{ij})-U_j\frac{\partial(\bar{\varrho}\tilde{u}_i)}{\partial x_j}=\frac{1}{Re}\frac{\partial}{\partial x_j}(\tilde{t}_{ij}+\tau_{ij}),\\
&\frac{D^A}{Dt}(\bar{\varrho}\tilde{e})+\frac{\partial}{\partial x_j}(\bar{\varrho}\tilde{e}\tilde{u}_j+\bar{p}\tilde{u}_j)-U_j\frac{\partial(\bar{\varrho}\tilde{e})}{\partial x_j}=\\
&\qquad=\frac{1}{Re}\frac{\partial}{\partial x_j}\left[(\tilde{t}_{ij}+\tau_{ij})\tilde{u}_i+\frac{\kappa}{\kappa-1}\left(\frac{\mu}{Pr}+\frac{\mu_t}{Pr_t}\right)\frac{\partial}{\partial x_j}\left(\frac{\bar{p}}{\bar{\varrho}}\right)\right],
\end{aligned}\tag{1}$$

where $i,j=1,2$, $\bar{\varrho}$ and $\bar{p}$ are dimensionless time-averaged values of density and pressure, $\tilde{u}_i$ are dimensionless mass-averaged Cartesian components of velocity vector, $\tilde{e}$ is mass-averaged energy, Re is the Reynolds number, Pr is the Prandtl number, μ and μ_t are dimensionless dynamic and turbulent viscosities and U_j are dimensionless components of the mesh velocity. The turbulent Prandtl number for flow around flat plate is $Pr_t=0.89$. Furthermore, the dimensionless mass-averaged stress tensor and the Reynolds stress tensor are given by

$$\tilde{t}_{ij}=2\mu\bar{S}_{ij},\ \tau_{ij}=2\mu_t\bar{S}_{ij},$$

where

$$\bar{S}_{ij}=\frac{1}{2}\left(\frac{\partial\tilde{u}_i}{\partial x_j}+\frac{\partial\tilde{u}_j}{\partial x_i}\right)-\frac{1}{3}\delta_{ij}\frac{\partial\tilde{u}_k}{\partial x_k}.$$

The equation of state for ideal gas is considered as

$$\bar{p}=(\kappa-1)\left[\bar{\varrho}\tilde{e}-\frac{1}{2}\bar{\varrho}\sum_{i=1}^{2}\tilde{u}_i^2\right].$$

Note that the symbol $\frac{D^A}{Dt}$ denotes the ALE derivative [6].

To include the influence of turbulent fluctuations on the mean flow a one-equation turbulence model of Spalart and Allmaras [7] is used. This turbulent model was designed specifically for aerospace applications (external flows) and therefore it seems to be an appropriate choice for the problem considered in this paper, which is described in section 5. The model is given by the transport equation for the dimensionless eddy viscosity $\tilde{\nu}$ written in the dimensionless ALE form as

$$\begin{aligned}
\frac{D^A(\bar{\varrho}\tilde{\nu})}{Dt}+\frac{\partial(\bar{\varrho}\tilde{\nu}\tilde{u}_j)}{\partial x_j}-U_j\frac{(\partial\bar{\varrho}\tilde{\nu})}{\partial x_j}=\frac{1}{Re}\frac{1}{\sigma}\left[\frac{\partial}{\partial x_j}\left((\mu+\bar{\varrho}\tilde{\nu})\frac{\partial\tilde{\nu}}{\partial x_j}\right)+\bar{\varrho}c_{b2}\frac{\partial\tilde{\nu}}{\partial x_j}\frac{\partial\tilde{\nu}}{\partial x_j}\right]+\\
+c_{b1}\bar{\varrho}\tilde{S}\tilde{\nu}-\frac{1}{Re}c_{w1}f_w\frac{1}{\bar{\varrho}}\left(\frac{\bar{\varrho}\tilde{\nu}}{D}\right)^2
\end{aligned}\tag{2}$$

and completed by the following relations

$$\mu_t=\bar{\varrho}\tilde{\nu}f_{v1},\ \ \tilde{S}=\bar{\Omega}+\frac{1}{Re}\frac{\tilde{\nu}}{\kappa^2D^2}f_{v2},\ \ f_w=g\left(\frac{1+c_{w3}^6}{g^6+c_{w3}^6}\right)^{\frac{1}{6}},\ \ g=r+c_{w2}\left(r^6-r\right),$$

$$r=\min\left(\frac{\tilde{\nu}}{Re\,\tilde{S}\kappa^2D^2},10\right),\ \ f_{v1}=\frac{\chi^3}{\chi^3+c_{v1}^3},\ \ \chi=\frac{\tilde{\nu}}{\nu},\ \ f_{v2}=1-\frac{\chi}{1+\chi f_{v1}}$$

with commonly used constants $c_{b1} = 0.1355,\ c_{b2} = 0.622,\ \sigma = \frac{2}{3},\ \kappa = 0.41,\ c_{w1} = \frac{c_{b1}}{\kappa^2} + \frac{1+c_{b2}}{\sigma},\ c_{w2} = 0.3,\ c_{w3} = 2.0,\ c_{v1} = 7.1$, D is the distance to the nearest wall and $\bar{\Omega}$ is the magnitude of vorticity.

The non-linear system of Favre-averaged Navier-Stokes equations (1) and the transport equation for eddy viscosity (2) are numerically solved as a single coupled system, which can be written in a dimensionless compact flux vector form as follows

$$\frac{D^A \boldsymbol{w}}{Dt} + \sum_{j=1}^{2} \left(\frac{\partial}{\partial x_j} \boldsymbol{f}_j(\boldsymbol{w}) - U_j \frac{\partial \boldsymbol{w}}{\partial x_j} \right) = \frac{1}{Re} \sum_{j=1}^{2} \frac{\partial}{\partial x_j} \boldsymbol{f}_j^v(\boldsymbol{w}, \nabla \boldsymbol{w}) + \boldsymbol{p}(\boldsymbol{w}, \nabla \boldsymbol{w}), \tag{3}$$

where $\boldsymbol{w}$ is the vector of flow variables, $\boldsymbol{f}_j(\boldsymbol{w})$ are the inviscid fluxes, $\boldsymbol{f}_j^v(\boldsymbol{w}, \nabla \boldsymbol{w})$ are the viscous fluxes and $\boldsymbol{p}(\boldsymbol{w}, \nabla \boldsymbol{w})$ is the production term. The vectors take the form

$$\boldsymbol{w} = \begin{bmatrix} \bar{\varrho} \\ \bar{\varrho}\tilde{u}_1 \\ \bar{\varrho}\tilde{u}_2 \\ \bar{\varrho}\tilde{e} \\ \bar{\varrho}\tilde{\nu} \end{bmatrix},\ \boldsymbol{f}_1(\boldsymbol{w}) = \begin{bmatrix} \bar{\varrho}\tilde{u}_1 \\ \bar{\varrho}\tilde{u}_1^2 + \bar{p} \\ \bar{\varrho}\tilde{u}_1\tilde{u}_2 \\ \tilde{u}_1(\bar{\varrho}\tilde{e} + \bar{p}) \\ \bar{\varrho}\tilde{\nu}\tilde{u}_1 \end{bmatrix},\ \boldsymbol{f}_2(\boldsymbol{w}) = \begin{bmatrix} \bar{\varrho}\tilde{u}_2 \\ \bar{\varrho}\tilde{u}_1\tilde{u}_2 \\ \bar{\varrho}\tilde{u}_2^2 + \bar{p} \\ \tilde{u}_2(\bar{\varrho}\tilde{e} + \bar{p}) \\ \bar{\varrho}\tilde{\nu}\tilde{u}_2 \end{bmatrix},$$

$$\boldsymbol{f}_1^v(\boldsymbol{w}, \nabla \boldsymbol{w}) = \begin{bmatrix} 0 \\ \tilde{t}_{11} + \tau_{11} \\ \tilde{t}_{12} + \tau_{12} \\ \sum_{i=1}^{2} \tilde{u}_i(\tilde{t}_{i1} + \tau_{i1}) + \frac{\kappa}{\kappa - 1} \left(\frac{\mu}{Pr} + \frac{\mu_t}{Pr_t} \right) \frac{\partial}{\partial x_1} \left(\frac{\bar{p}}{\bar{\varrho}} \right) \\ \frac{1}{\sigma} (\mu + \bar{\varrho}\tilde{\nu}) \frac{\partial \tilde{\nu}}{\partial x_1} \end{bmatrix},$$

$$\boldsymbol{f}_2^v(\boldsymbol{w}, \nabla \boldsymbol{w}) = \begin{bmatrix} 0 \\ \tilde{t}_{12} + \tau_{12} \\ \tilde{t}_{22} + \tau_{22} \\ \sum_{i=1}^{2} \tilde{u}_i(\tilde{t}_{i2} + \tau_{i2}) + \frac{\kappa}{\kappa - 1} \left(\frac{\mu}{Pr} + \frac{\mu_t}{Pr_t} \right) \frac{\partial}{\partial x_2} \left(\frac{\bar{p}}{\bar{\varrho}} \right) \\ \frac{1}{\sigma} (\mu + \bar{\varrho}\tilde{\nu}) \frac{\partial \tilde{\nu}}{\partial x_2} \end{bmatrix},$$

$$\boldsymbol{p}(\boldsymbol{w}, \nabla \boldsymbol{w}) = \begin{bmatrix} 0 \\ 0 \\ 0 \\ 0 \\ \frac{1}{Re} \frac{1}{\sigma} \bar{\varrho} c_{b2} \left(\frac{\partial \tilde{\nu}}{\partial x_1} \frac{\partial \tilde{\nu}}{\partial x_1} + \frac{\partial \tilde{\nu}}{\partial x_2} \frac{\partial \tilde{\nu}}{\partial x_2} \right) + c_{b1} \bar{\varrho} \tilde{S} \tilde{\nu} - \frac{1}{Re} c_{w1} f_w \frac{1}{\bar{\varrho}} \left(\frac{\bar{\varrho}\tilde{\nu}}{D} \right)^2 \end{bmatrix}.$$

3 DISCRETIZATION

The spatial discretization of equations (3) is performed using the discontinuous Galerkin finite element method (DGFEM), see for example [8], [9], [10]. Let $\mathcal{T}_h = \{\Omega_k : \bigcup_k \overline{\Omega}_k = \overline{\Omega} \ \wedge \ \bigcap_k \Omega_k = \emptyset,\ k = 1, \ldots, K\}$ be a triangulation of the time-varying computational domain $\Omega(t) \in \mathcal{R}^2$ boundary of which is denoted by $\partial\Omega$. Note that each element may vary in time, i.e. $\Omega_k = \Omega_k(t)$. Let Γ^{int} and $\Gamma^b \subset \partial\Omega$ be the sets of interior and boundary edges of elements in $\mathcal{T}_h$. In order to discretize the non-linear system of equations (3) the infinite dimensional function space is replaced by the finite dimensional function space $\mathbf{S}_h = [S_h]^4$, where

$$S_h = \{g \in L^2(\Omega) :\ g|_{\Omega_k} \in \mathcal{P}^q(\Omega_k) \quad \forall \Omega_k\} \tag{4}$$

and $\mathcal{P}^q(\Omega_k)$ is the space of polynomials of degree q on Ω_k.

Multiplying the system of equations (3) by a test function $\boldsymbol{v} \in \mathbf{S}_h$, integrating it over Ω_k and applying Green's theorem and the Reynolds transport theorem, the following integral identity is obtained

$$\begin{aligned}\frac{\mathrm{d}}{\mathrm{d}t}\int_{\Omega_k} \boldsymbol{w}\cdot\boldsymbol{v}\,\mathrm{d}\Omega\; &- \int_{\Omega_k}\sum_{j=1}^{2}(\boldsymbol{f}_j(\boldsymbol{w})-U_j\boldsymbol{w})\cdot\frac{\partial \boldsymbol{v}}{\partial x_j}\,\mathrm{d}\Omega + \oint_{\partial\Omega_k}\sum_{j=1}^{2}(\boldsymbol{f}_j(\boldsymbol{w})-U_j\boldsymbol{w})n_j\cdot\boldsymbol{v}\,\mathrm{d}l = \\ &= \frac{1}{Re}\oint_{\partial\Omega_k}\sum_{j=1}^{2}\boldsymbol{f}_j^v(\boldsymbol{w},\nabla\boldsymbol{w})n_j\cdot\boldsymbol{v}\,\mathrm{d}l - \frac{1}{Re}\int_{\Omega_k}\sum_{j=1}^{2}\boldsymbol{f}_j^v(\boldsymbol{w},\nabla\boldsymbol{w})\cdot\frac{\partial\boldsymbol{v}}{\partial x_j}\,\mathrm{d}\Omega + \\ &+ \int_{\Omega_k}\boldsymbol{p}(\boldsymbol{w},\nabla\boldsymbol{w})\cdot\boldsymbol{v}\,\mathrm{d}\Omega.\end{aligned}$$

The key part of the method is the approximation of curve integrals. In case of the discontinuous Galerkin method, this procedure is analogous to the finite volume approach. In particular, the inviscid fluxes are evaluated as

$$\sum_{j=1}^{2}\boldsymbol{f}_j(\boldsymbol{w})n_j \approx \boldsymbol{\mathcal{H}}(\boldsymbol{w}^+,\boldsymbol{w}^-)\;\text{ on }\;\Gamma^{int},$$

$$\sum_{j=1}^{2}\boldsymbol{f}_j(\boldsymbol{w})n_j \approx \boldsymbol{\mathcal{H}}(\boldsymbol{w}^b,\boldsymbol{w}^-)\;\text{ on }\;\Gamma^{b},$$

where $\boldsymbol{n} = [n_1, n_2]^T$ is the outer unit normal vector, $\boldsymbol{w}^-$ and $\boldsymbol{w}^+$ are respectively the left and right limits of $\boldsymbol{w}$ on the edges of $\Gamma^{int}\cup\Gamma^b$ and $\boldsymbol{w}^b$ is the value of $\boldsymbol{w}$ at the boundary $\partial\Omega$ evaluated out of the prescribed boundary condition. As the numerical flux $\boldsymbol{\mathcal{H}}$, the Lax-Friedrichs flux, see [11],

$$\boldsymbol{\mathcal{H}}(\boldsymbol{w}^+,\boldsymbol{w}^-) = \frac{1}{2}\left(\sum_{j=1}^{2}\left(\boldsymbol{f}_j(\boldsymbol{w}^+)+\boldsymbol{f}_j(\boldsymbol{w}^-)\right)n_j - \lambda\left(\boldsymbol{w}^+-\boldsymbol{w}^-\right)\right)$$

is considered, where $\lambda = |\sum_{j=1}^{2}\tilde{u}_j n_j| + \bar{a}$ is the maximal eigenvalue and $\bar{a} = \sqrt{\kappa\bar{p}/\bar{\varrho}}$ is the local speed of sound. Similarly, the viscous fluxes are evaluated using appropriate numerical fluxes. In the present paper, the approximation known as interior penalty method is chosen, see [10] for more details.

The discontinuous Galerkin method is stable under the L^2-norm, however it does not provide TVD stability. For this reason the undesirable oscillations can occurs in the presence of shock waves or in the regions with high gradients. In these cases, a small amount of the artificial viscosity is added into the right hand side of the system of equations (3) through the term

$$\epsilon\frac{\partial^2\boldsymbol{w}}{\partial x_j\partial x_j}, \tag{5}$$

where $\epsilon = I_s\frac{\lambda h}{q}$ and λ is the maximum eigenvalue, h is the minimum element diameter, q is the degree of basis polynomials and I_s is a parameter determined by the shock wave indicator. In this paper, the shock wave indicator proposed in [12] is chosen. Following [12] the density $\bar{\varrho}$ is expressed as a linear combination of basis functions up to degree q and up to degree $(q-1)$

$$\bar{\varrho}_k = \sum_{i=1}^{N(q)}\bar{\varrho}_{k,i}\varphi_{k,i}(\boldsymbol{x}), \qquad \hat{\bar{\varrho}}_k = \sum_{i=1}^{N(q-1)}\bar{\varrho}_{k,i}\varphi_{k,i}(\boldsymbol{x}),$$

respectively. Consequently, the value of the smoothness indicator is defined for each element Ω_k as

$$S_{e,k} = \frac{(\bar{\varrho}_k - \hat{\bar{\varrho}}_k,\ \bar{\varrho}_k - \hat{\bar{\varrho}}_k)}{(\bar{\varrho}_k,\ \bar{\varrho}_k)},$$

where $(\cdot,\ \cdot)$ is the standard L^2 inner product on Ω_k. Finally, the value I_s is set to

$$I_s = \begin{cases} 0 & \text{if } \ s_{e,k} < s_0 - \gamma, \\ \frac{1}{2}\left[1 + \sin\left(\frac{\pi(s_{e,k}-s_0)}{2\gamma}\right)\right] & \text{if } \ s_0 - \gamma \le s_{e,k} \le s_0 + \gamma, \\ 1 & \text{if } \ s_{e,k} > s_0 + \gamma, \end{cases}$$

where $s_{e,k} = \log_{10} S_{e,k},\ s_0 = 1/q^4$ and γ is a chosen constant. See [12] for more details.

Let $\boldsymbol{w}_k$ be the restriction of $\boldsymbol{w}$ on Ω_k and let $\varphi_{k,i} \in \mathcal{P}^q(\Omega_k)$ be the i-th basis function on Ω_k. In this study, linear Lagrange polynomials are chosen as the basis functions $\varphi_{k,i}$. The m-th component w_k^m, $m = 1, 2, ..., 4$, of $\boldsymbol{w}_k$ can be expressed as a linear combination of basis functions as follows

$$w_k^m(\boldsymbol{x}, t) = \sum_{i=1}^{N(q)} w_{k,i}^m(t)\varphi_{k,i}(\boldsymbol{x}). \tag{6}$$

Expanding the solution as a linear combination of basis functions and evaluating the volume and curve integrals using Gaussian quadrature of appropriate order the following system of ordinary differential equations is obtained

$$\frac{\mathrm{d}(\mathbf{MW})}{\mathrm{d}t} = \mathbf{R}(\mathbf{W}), \tag{7}$$

where the vector $\mathbf{W}$ consists of unknown coefficients of linear combination (6) and $\mathbf{M}$ is the mass matrix.

The time integration of (7) is performed using the implicit backward Euler method and the resulting system of non-linear algebraic equations is solved by Newton's method

$$\begin{aligned} &\boldsymbol{W}^{s=0} = \boldsymbol{W}^n, \\ &\left[\frac{\boldsymbol{M}^{n+1}}{\Delta t} - \frac{\partial \boldsymbol{R}}{\partial \boldsymbol{W}}(\boldsymbol{W}^s)\right]\Delta \boldsymbol{W} = \boldsymbol{R}(\boldsymbol{W}^s) - \frac{\boldsymbol{M}^{n+1}\boldsymbol{W}^s - \boldsymbol{M}^n\boldsymbol{W}^n}{\Delta t}, \\ &\boldsymbol{W}^{s+1} = \boldsymbol{W}^s + \Delta \boldsymbol{W}, \\ &\boldsymbol{W}^{s+1} \longrightarrow \boldsymbol{W}^{n+1}. \end{aligned} \tag{8}$$

The system of linear equations (8) is solved iteratively using the GMRES method with the block diagonal Jacobi preconditioner.

4 VALIDATION OF THE IN-HOUSE CFD CODE

Before moving on to the numerical simulation of the fluid flow through the simplified blade cascade, which is the central target of the paper, it is necessary to validate the developed CFD code. Since the experimental data for the simplified blade cascade is not available yet, two test problems commonly studied in literature are chosen, see [13].

Firstly, comparisons are made for simulations of an inviscid compressible steady fluid flow around the NACA0012 airfoil at Mach number 0.8 for angles of attack varying between $\pm 4°$. The computational mesh with 10905 elements is shown in Figure 1 in the vicinity of the airfoil.

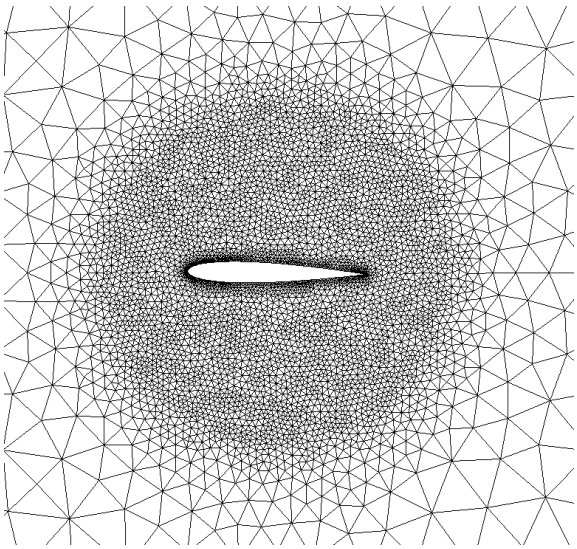

Figure 1: Computational mesh in the vicinity of the NACA0012 airfoil.

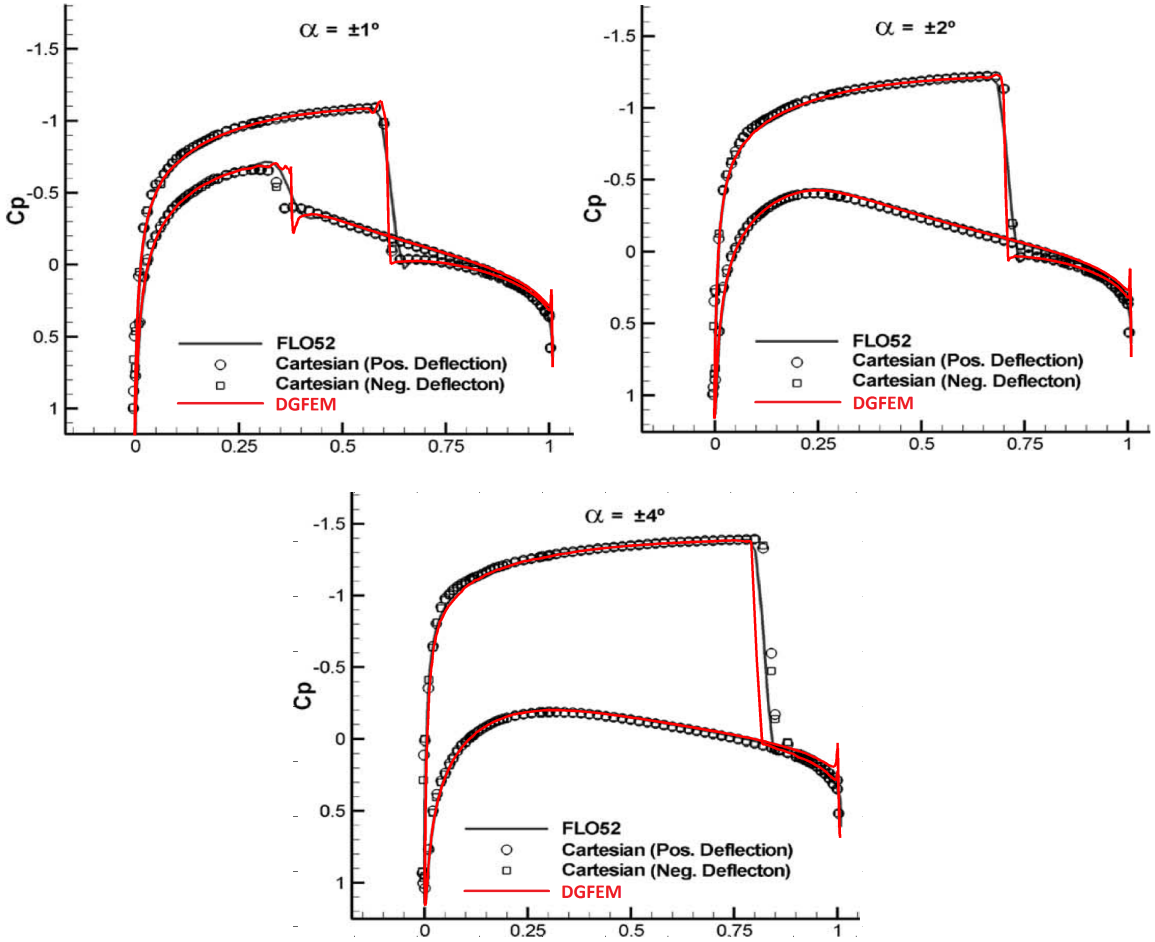

Figure 2: Distribution of c_p coefficient along the airfoil chord for various angles of attack α.

The resulting c_p coefficient on the surface of the airfoil computed by the developed DGFEM code (colored red) along with the data taken from [13] (colored black) is shown in Figure 2.

The second test case for validation is an inviscid compressible unsteady fluid flow around oscillating NACA0012 airfoil for a free stream Mach number $M_\infty = 0.755$. The instantaneous

motion of the airfoil is given as a function of time

$$\alpha(t) = \alpha_m + \alpha_o \sin(\omega\, t),$$

which defines the angle of tilt of the airfoil. Here the mean angle $\alpha_m = 0.016°$ and the amplitude of oscillation $\alpha_o = 2.51°$. The angular velocity is defined as $\omega = 2ku_\infty/c$, where reduced frequency $k = 0.0814$, profile chord length $c = 1$ and u_∞ is a free-stream velocity. The coordinates of reference point of rotation are $x_{ref} = [0.25, 0]$. The Figure 3 show a comparison of obtained numerical results (red) by the developed code with the results published in [13] and [14] (black). A reasonably good agreement is apparent from both of the test problems, which confirms a correct implementation of the implicit DGFEM solver along with the ALE approach.

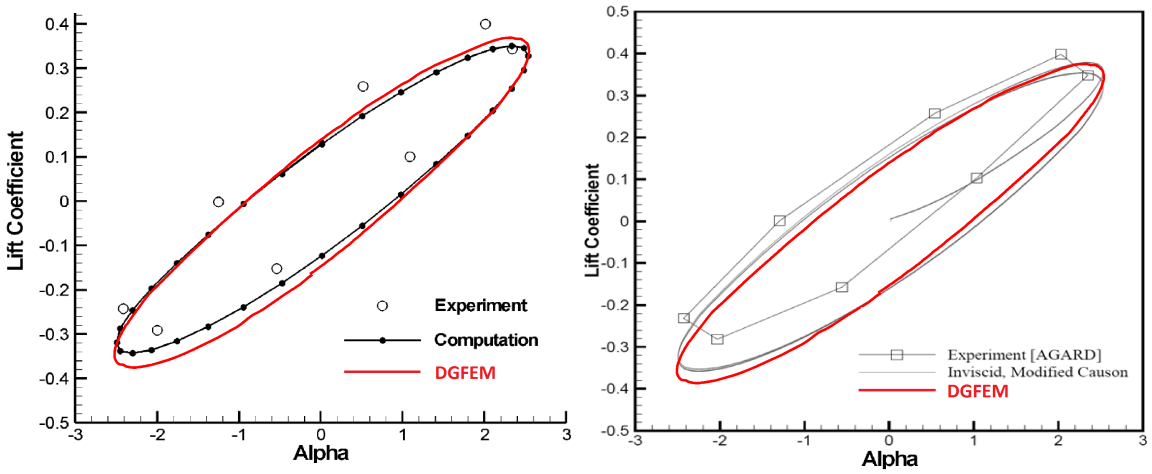

Figure 3: Dependence of the lift coefficient c_L on the angle of the airfoil. Comparison with the numerical and experimental results published in [13] (left) and [14] (right).

5 NUMERICAL RESULTS

The developed in-house CFD software based on the discontinuous Galerkin method was used to simulate compressible viscous fluid flow through a simplified blade cascade with prescribed harmonic motion. The geometric configuration of the simplified blade cascade and the angle of attack of the flow were adopted from [4], test case no. 3, where it was experimentally studied. The only difference is that the thin airfoils of the test cascade from [4] were replaced by 3 millimetres thick flat plates. The geometric configuration of the simplified test cascade is shown in Figure 4.

The considered two-dimensional computational domain and the corresponding unstructured triangular mesh with 11932 elements is shown in Figure 5 (left). The detailed view of the mesh in the vicinity of the three flat plates is shown in Figure 5 (right). For the computation of the deformed coordinates of mesh nodes, the blending function approach is used, see [15], [16]. In this paper the blending function is generalized for three independently moving flat plates, Figure 4. Let us look at the computation of the deformed mesh in more detail. Let $\boldsymbol{x}_0$ denote the vector of initial coordinates of all mesh nodes. For each blade ($i = 1, 2, 3$) the vector $\boldsymbol{x}_0$ of initial coordinates is transformed into a new vector $\boldsymbol{y}_i$ using the following formula:

$$\boldsymbol{y}_i = \boldsymbol{p}_i + \mathbf{T}(\alpha)_i \boldsymbol{x}_0, \tag{9}$$

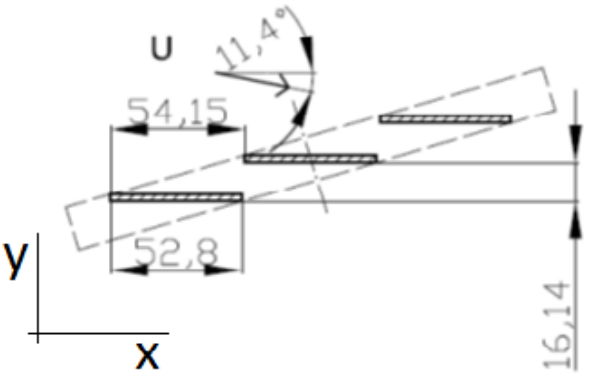

Figure 4: The geometric configuration of the simplified cascade which consists of three oscillating flat plates. The dimensions are in millimetres. The width of the plates is 80 mm.

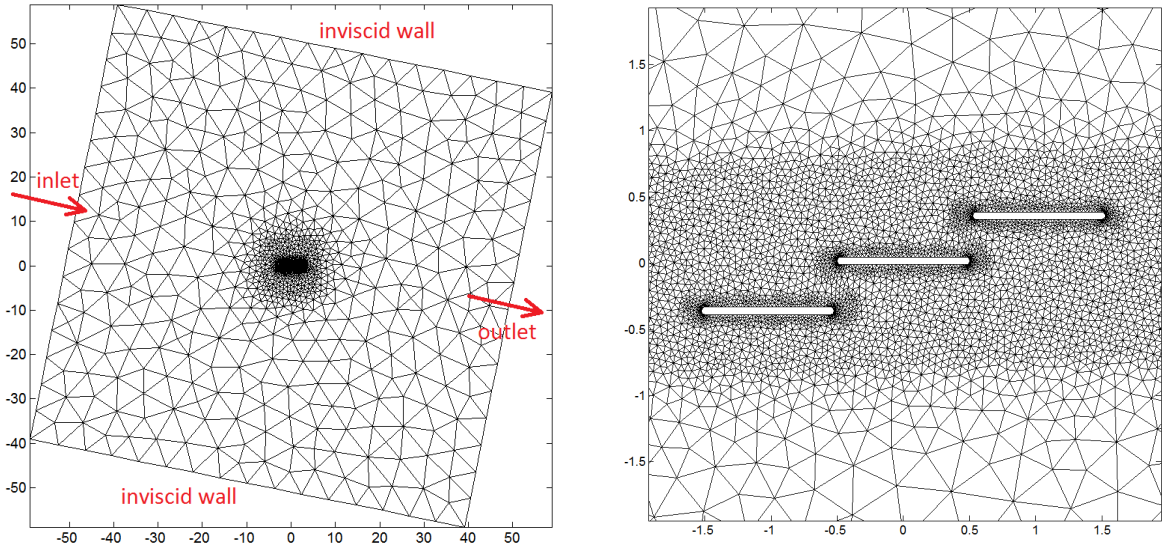

Figure 5: Computational domain and triangular mesh (left), computational mesh in the vicinity of simplified cascade (right).

where $\boldsymbol{p}_i = \boldsymbol{p}_i(t)$ is the time dependent translation vector and $\mathbf{T}(\alpha)_i = \mathbf{T}(\alpha(t))_i$ is the time dependent rotation matrix of i-th blade. The vector $\boldsymbol{x} = \boldsymbol{x}(t)$ of new coordinates is computed by applying the blending function b_i as follows

$$\boldsymbol{x} = \frac{1}{n}\sum_{i=1}^{n}(b_i(\boldsymbol{x}_0)\boldsymbol{x}_0 + (1 - b_i(\boldsymbol{x}_0))\boldsymbol{y}_i). \tag{10}$$

The key part of this algorithm is to determine the blending functions b_i, which must satisfy two basic properties:

1. $b_i = 0$ on the boundary of the i-th blade,
2. $b_i = 1$ on the boundary of the j-th blade and on the boundary of the computational domain.

A blending function b_i, which fulfils the two properties, can be obtained by solving the equation

$$\frac{\partial^2 b_i}{\partial x^2} + \frac{\partial^2 b_i}{\partial y^2} = 0, \tag{11}$$

equipped with the boundary condition $b_i = 0$ on the i-th blade and $b_i = 1$ on the rest of the boundary. The solution to the boundary value problem (11) for the considered three flat plates defined in Figure 4 is shown in Figure 6.

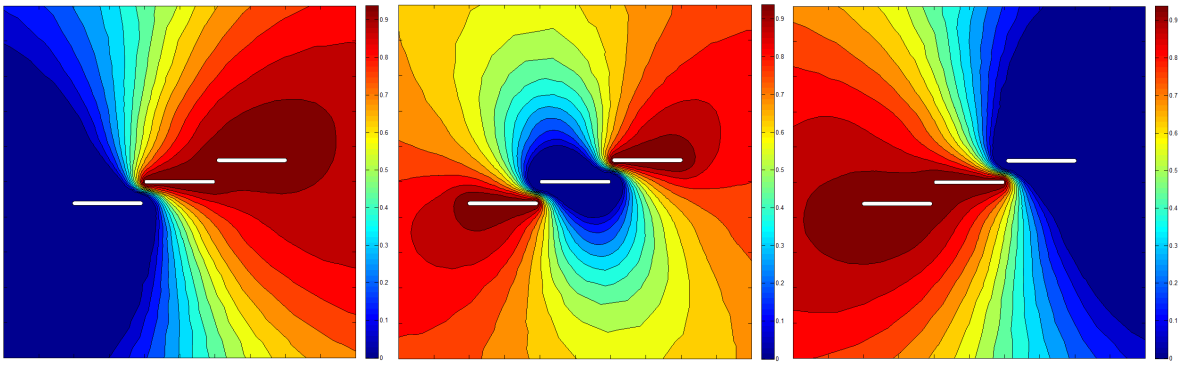

Figure 6: Solution to the boundary value problem (11) for bottom plate (left), middle plate (middle) and top plate (right) in viscinity of the three flat plates.

Each plate performs kinematic harmonic motion in y-direction $y = A\sin(2\pi ft + \phi)$ with an inter-blade phase angle $\phi = +\varphi$ for the upper plate, $\phi = 0$ for the middle plate and $\phi = -\varphi$ for the bottom plate. The amplitude and the frequency of the harmonic motion is $A = 0.003\,\mathrm{m}$ and $f = 20\,\mathrm{Hz}$, respectively. In [5], this problem was solved only for $\varphi = \pi/2$. Here, the analysis of the problem is extended to angles $\varphi = \{-3/4\pi, -1/2\pi, -1/4\pi, 1/4\pi, 1/2\pi, 3/4\pi, \pi\}$.

At the inlet of the computational domain, see Figure 5, the stagnation pressure $\bar{p}_{01} = 101325\,\mathrm{Pa}$, the stagnation temperature $\bar{T}_{01} = 293.15\,\mathrm{K}$ and the angle of attack $\alpha = 11.4°$ were prescribed. At the outlet, the static pressure $\bar{p}_2 = 95520\,\mathrm{Pa}$ was prescribed. The value of $\bar{p}_2$ was calculated out of the free stream velocity $\tilde{u}_\infty = 100\,\mathrm{ms}^{-1}$ under the consideration of standard sea level air conditions.

Figure 7 shows phase diagrams where the y-component of aerodynamic force acting on the middle plate is plotted depending on y-component of the displacement for various inter-blade phase angles φ. The obtained y-components of aerodynamic forces acting on the middle plate were analysed for all inter-blade face angles and consequently the aerodynamic damping parameter

$$\sigma = -\frac{c_w}{\pi A^2}$$

was determined. The variable

$$c_w = \int F_y dy$$

denotes the work of aerodynamic forces acting on the middle plate preformed during one cycle of harmonic motion with time period T. The resulting aerodynamic damping parameter σ depending on inter-blade face angle φ is shown in Figure 8. The parameter σ has the following meaning. If the value of σ is positive, than the kinetic energy of the flat plate is transmitted to the flow and the oscillation is damped. In this case the flutter most likely does not occur. If the value of σ is negative, than the kinetic energy of the flow is transmitted to the flat plate and thus the flutter phenomena can occur.

6 CONCLUSION

The CFD solver based on the discontinuous Galerkin method was developed for the numerical solution of compressible viscous flow problems in domains with moving boundaries. The

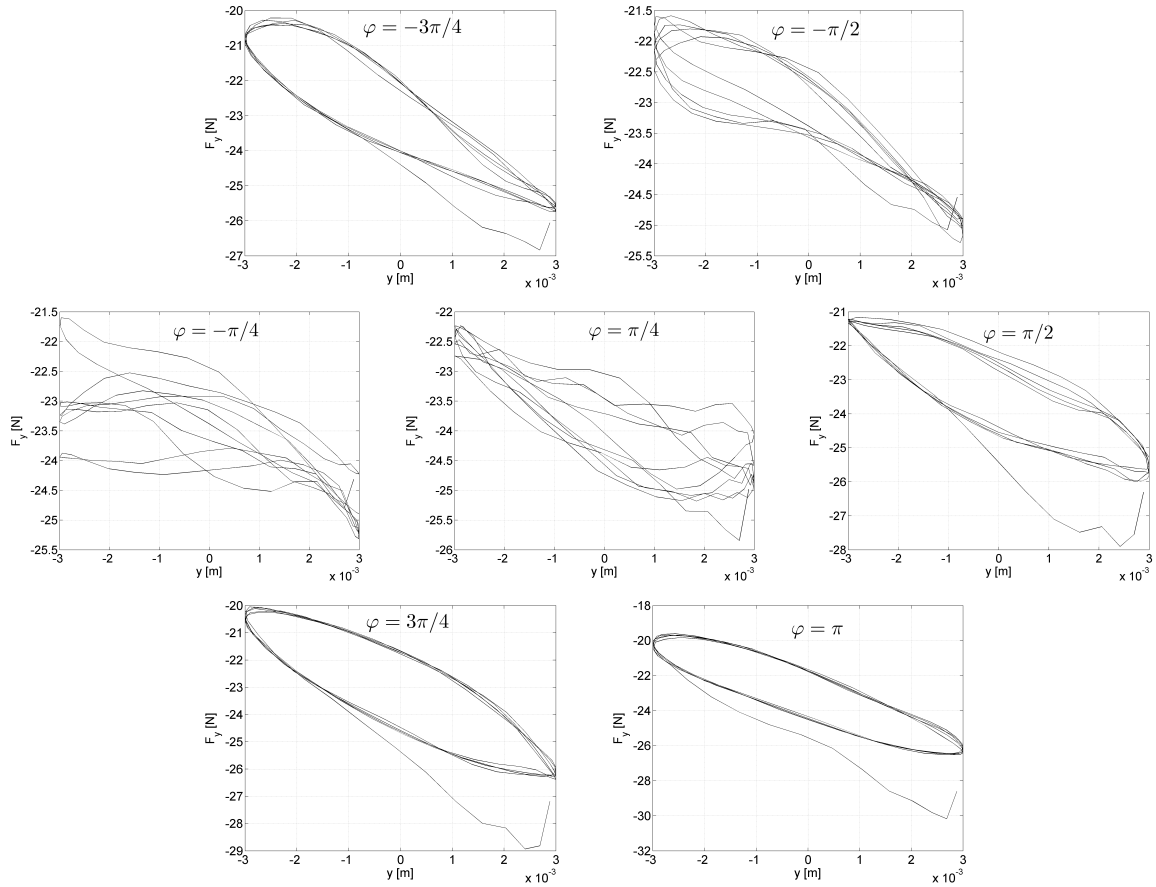

Figure 7: Phase diagrams of y-component of aerodynamic force acting on the middle plate depending on y-component of displacement for various inter-blade phase angles φ.

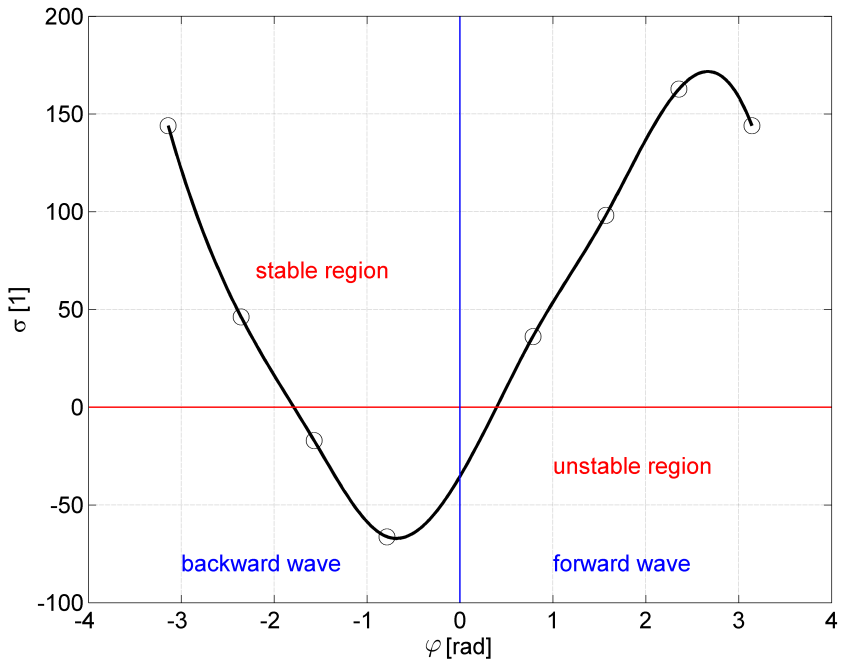

Figure 8: Aerodynamic damping parameter σ depending on the inter-blade phase angle φ.

solver was validated on two test problems and consequently it was applied to numerical simulation of compressible viscous fluid flow through the simplified blade cascade formed by three flat plates with prescribed harmonic motion.

The presented results of flow field were analysed with regard to the flutter occurrence. The theory of the simplified blade cascade [3] as well as the results presented in this paper, Figure 8, suggest that the flutter occurs for the backward travelling wave mode. An experimental validation of results presented in this paper is planned in the near future in the Institute of Thermomechanics of the Czech Academy of Sciences.

ACKNOWLEDGEMENTS

The authors appreciate the kind support by the grant GA16-04546S *"Aero-elastic couplings and dynamic behaviour of rotational periodic bodies"* of the Czech Science Foundation.

REFERENCES

[1] H.M. Owens, W.E. Trumpler, Mechanical Design and Testing of Long Steam Turbine Blanding. *ASME Paper*, **49-A-64**, 1949.

[2] E.K. Armstrong, R.E. Stevenson, Some Practical Aspect of Compressor Blade Vibration. *Journal of the Royal Aeronautical Society*, **64** (591), 117-130, 1960.

[3] R. Kielb, J. Barter, O. Chernycheva, T. Fransson, Flutter of low pressure turbine blades with cyclic symmetric modes: A preliminary design method. *Journal of Turbomachinery, Transactions of the ASME*, **126**, 306-309, 2004.

[4] D. Schlafli, *Experimental investigation of transient flow in oscillating ring lattices*, Ph.D. Thesis no. 800, Lausanne, 1989. (in German)

[5] J. Vimmr, O. Bublík, H. Prausová, J. Hála, L. Pešek, Numerical simulation of fluid flow through simplified blade cascade with prescribed harmonic motion using discontinuous Galerkin method. *EPJ Web of Conferences*, 2017. (in press)

[6] M. Feistauer, J. Česenek, Space-Time Discontinuous Galerkin Finite Element Method for Convection-Diffusion Problems and Compressible Flow. *Numerical Methods and Applications, Lecture Notes in Computer Science*, **6046**, 1-13, 2011.

[7] P.R. Spalart, S.R. Allmaras, A One-Equation Turbulence Model for Aerodynamic Flows. *AIAA Paper*, **92-439**, 1992.

[8] W.H. Reed, T.R. Hill, Triangular mesh methods for the neutron transport equation. *Los Alamos Scientific Laboratory Report*, **LA-UR-73-479**, 1973.

[9] B. Cockburn, C.-W. Shu, Runge-Kutta Discontinuous Galerkin Methods for Convection-Dominated Problems. *Journal of Scientific Computing*, **16** (3), 173-261, 2001.

[10] V. Dolejší, M. Holík, J. Hozman, Efficient solution strategy for semi-implicit discontinuous Galerkin discretization of the Navier-Stokes equation. *Journal of Computational Physics*, **230** (11), 4176-4200, 2011.

[11] E.F. Toro, *Riemann Solvers and Numerical Methods for Fluid Dynamics*. Springer, Heidelberg, 1999.

[12] P.-O. Persson, J.Peraire, Sub-Cell Shock Capturing for Discontinuous Galerkin Methods. *44th AIAA Aerospace Sciences Meeting and Exhibit*, Reno, Nevada, January 9-12, 2006.

[13] D.J. Kirshman, F. Liu, Flutter prediction by an Euler method on non-moving Cartesian grids with gridless boundary conditions. *Computers and Fluids*, **35** (6), 571-586, 2006.

[14] J. Fürst, K. Kozel, P. Furmánek, High order finite volume schemes for numerical solution of 2D and 3D transonic flows. *Kybernetika*, **45** (4), 567-579, 2009.

[15] P.-O. Persson, J. Bonet, J. Peraire, Discontinuous Galerkin solution of the Navier-Stokes equations on deformable domains. *Computer Methods in Applied Mechanics and Engineering*, **198** (17-20), 1585-1595, 2009.

[16] O. Bublík, J. Vimmr, A. Jonášová, Comparison of discontinuous Galerkin time integration schemes for the solution of flow problems with deformable domains. *Applied Mathematics and Computation*, **267**, 329-340, 2015.